International Journal of Thermal Sciences 48 (2009) 1138–1150

Contents lists available at ScienceDirect

International Journal of Thermal Sciences

www.elsevier.com/locate/ijts

Longitudinal heat conduction study of a uniform power density apparatus for the experimental determination of the heat transfer coefficient

E. Da Riva [a], J.M. Corberán [b,*], E.L. Cuadros [b]

[a] Dipartimento di Fisica Tecnica, Università degli Studi di Padova, Via Venezia 1, 35131 Padova, Italy
[b] Departamento de Termodinámica Aplicada, Universidad Politécnica de Valencia, Camino de Vera s/n, 46022 Valencia, Spain

ARTICLE INFO

Article history:
Received 28 November 2007
Received in revised form 2 September 2008
Accepted 5 September 2008
Available online 21 October 2008

Keywords:
Longitudinal conduction
Heat transfer coefficient evaluation

ABSTRACT

A combined experimental and numerical analysis was performed to accurately evaluate the effect of longitudinal heat conduction along an aluminium test section on the local heat transfer coefficient (HTC) experimental determination. The test section contains a rectangular channel with fins typical of compact heat exchangers. The hydraulic diameter of the channel is around 2 mm. The fluid stream is heated by flat electrical resistances clamped to the outer walls of the test section. The test section contains four zones with different fin pads each, in order to be able to generate data for several geometries at the same time at exactly the same mass flow rate.

It was found that longitudinal conduction can lead to a quite uneven distribution of the heat flux to the fluid at the beginning and end of each zone of the test section. Three phenomena were found to be the cause for the observed uneven heat distribution, i.e. the longitudinal gradient of temperature along the wall induced by the fluid temperature rise, the presence of heated and non-heated zones, and the stepwise non-uniformity of the HTC along the test section induced where the fin pad changes.

The study has shown that the elementary data reduction methodology, assuming that the surface power density generated by the electrical resistance and the heat flux density reaching the fluid are equal and uniform along the channel, is too far from the reality at the beginning and end of each zone of the test section, especially at low mass flow rates.

1. Introduction

Electrical resistances whose design assures a uniform surface power density are commonly employed to heat the fluid stream in the test sections used to experimentally evaluate the local heat transfer coefficient (HTC). Fig. 1 shows the cross section of the involved experimental set up. The elementary data reduction methodology is based on the assumption of negligible longitudinal conduction and perfect insulation. In this way, in each segment of the test section, the power transmitted to the fluid is assumed to be equal to the power generated electrically, which can be measured by a power transducer. Then, the local HTC can be computed by evaluating the difference between the wall and the fluid temperatures.

However, the temperature distribution along the test section results quite uneven along it provoking relatively strong heat conduction effects and therefore, redistribution of the heat flux to the fluid.

This problem has mainly been studied referring to microchannel heat sink cooling devices, where wall axial conduction effects can be rather strong because of their geometrical features, since the wall thickness is comparable to, or larger than, the hydraulic diameter of the channel.

Referring to the investigation by Tso and Mahulikar [1] into laminar flow in a 0.7 mm i.d. circular micro-channel, Herwig and Hausner [2] reported that not taking into account axial heat transfer could lead to a considerable bias in the interpretation of experimental results. In fact, in Tso and Mahulikar [1], the local computed values of the Nusselt number were significantly lower than the theoretical ones, and they also exhibited the unusual behaviour of decreasing with increasing local Reynolds number. Tso and Mahulikar explained their results by means of dissipation effects correlating their data with the Brinkman number. Herwig and Hausner [2] performed a CFD analysis of heat flux in the test section used in Tso and Mahulikar [1], and their results indicated that the fluid bulk temperature was not linearly distributed between the inlet and outlet values as assumed by Tso and Mahulikar [1]. Furthermore, Herwig and Hausner [2] reported that the data reduction performed with the numerically computed temperature distribution showed no unusual behaviour.

Fedorov and Viskanta [3], Qu and Mudawar [4] and Li et al. [5] conducted three-dimensional numerical analyses of heat transfer for the laminar flow ($Re = 140$) of water in a silicon rectangular

* Corresponding author.
E-mail address: corberan@ter.upv.es (J.M. Corberán).

1290-0729/$ – see front matter
doi:10.1016/j.ijthermalsci.2008.09.003

Nomenclature

A_1	primary channel area, $A_1 = 2(P + e_f)L$
A_2	secondary channel area, $A_2 = 2(fP - 1)e_f L$
A_w	wall cross section
c_p	fluid specific heat
D_h	hydraulic diameter of the channel between two fins
D_h^*	hydraulic diameter of the channel without fins
e_f	channel thickness (see Fig. 1)
e_w	wall thickness (see Fig. 1)
f	fins per meter of channel width
G	mass flux
h	heat transfer coefficient (HTC)
k_w	wall thermal conductivity
k_f	fluid thermal conductivity
k	turbulent kinetic energy
L	channel length
M	axial conduction number [6]
m	mass flow rate
P	heater and channel width (see Fig. 1)
P_1	half perimeter of the primary channel area, $P_1 = P + e_f$
P_{htr}	heating power for a single channel sector
q_h	electrical resistance heat flux density
Re	Reynolds number
Pr	Prandtl number
T_w	wall temperature
T_{bulk}	fluid bulk temperature

Greek symbols

ε	turbulent dissipation rate
η	fin effectiveness

Subscripts

in	instrument plate 1 (see Fig. 3)
out	instrument plate 3 (see Fig. 3)

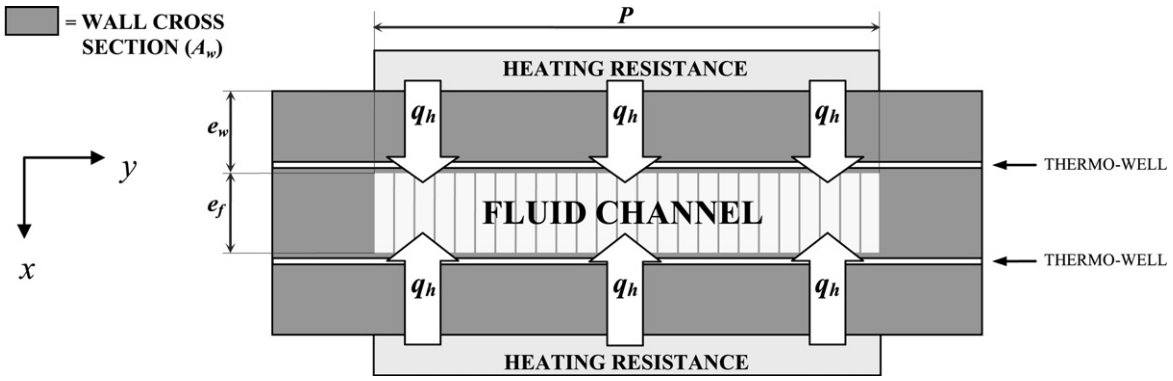

Fig. 1. Cross section of the test section.

57 μm × 180 μm micro-channel with the same geometry used in the experimental work by Kawano et al. [7]. The results obtained by Fedorov and Viskanta [3] indicated that the channel wall temperature along the flow direction was nearly uniform (except in the region close to the channel inlet where a large increase was observed), and the fluid bulk temperature distribution was not linear. However, Qu and Mudawar [4] performed their computation under the same conditions as Fedorov and Viskanta [3] and reported that a linear rise for both wall and fluid bulk temperature was a good approximation. Li et al. [5] explained this difference by noting that in Fedorov and Viskanta [3] the thermophysical properties were assumed to be temperature-dependent, while in Qu and Mudawar [4] they were not temperature-dependent. Li et al. [5] showed that both wall and fluid bulk temperatures vary almost linearly in the longitudinal direction, except at low flow rates.

In another numerical and experimental work by Qu and Mudawar [8] for laminar flow in a copper rectangular 231 μm × 713 μm micro-channel, performed assuming temperature-dependent fluid viscosity, the wall and fluid bulk temperatures were shown to vary linearly in the longitudinal direction.

All the reported numerical analyses [3–5,8] considered a single micro-channel as the computing domain, excluding the presence of inlet and outlet collectors. Moreover, in most cases [3–5] heat loss to the ambient was considered negligible.

Tiselj et al. [9] performed an experimental and numerical analysis focusing on the effect of axial conduction to evaluate heat transfer characteristics of water flowing through triangular silicon micro-channels with hydraulic diameter $D_h = 160$ μm heated by electrical resistances, in the range of Reynolds number $Re = 3.2–64$. All 17 micro-channels of the test section and the steel collectors were included in the computational domain of the "complete numerical model" developed. Furthermore, heat losses to the ambient were taken into account. Most of the results reported were obtained for a "reduced model" considering only a single channel as computing domain, yet indirectly taking into account of the collectors by imposing the value of axial heat flux obtained experimentally as a thermal boundary condition at the inlet and outlet. Computed wall and fluid temperature changed neither linearly nor monotonously along the channel and, next to the outlet, their gradients changed sign. The computed axial heat flux at the entrance of the channel acted in a direction opposite to fluid flow, then it changed sign next to the outlet. Moreover, the electrical resistances did not cover the entire length of the test section and the first derivative of the axial heat flux presented singular points in the positions corresponding to the electrical heater ends.

The effect of axial conduction in the wall in micro-channels was also investigated by Maranzana et al. [10] who examined the thermal structure of laminar flow between parallel plates by means of the axial conduction number M, already introduced by Peterson [6], defined as the ratio of the conductive heat flux to the convective one. Maranzana et al. [10] proved that for small Reynolds numbers, the wall heat flux density may become strongly non-uniform.

The present research is related with the experimental estimation of local HTC of boiling n-pentane along vertical channels with

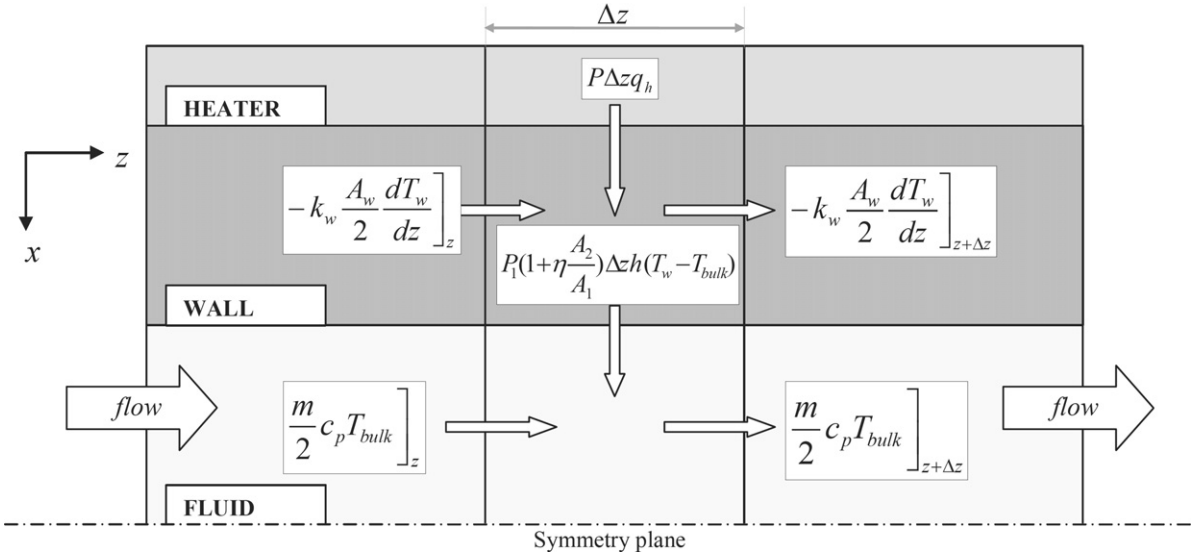

Fig. 2. Longitudinal section of wall and fluid cells.

internal fins. The hydraulic diameter of the channel with fins is around $D_h = 0.002$ m.

In the test section considered, heat is supplied by electrical mats and the wall temperature distribution is measured by numerous thermocouples inserted all along the wall, while fluid temperature and pressure are measured at the inlet and outlet, as well as in the middle of the test section.

The present study was performed to evaluate how longitudinal conduction affects the HTC evaluation in the employed test section. The test rig was operated under single phase flow conditions in order to generate high temperature gradients along the heat exchanger, and thus increase the longitudinal conduction effect and characterise it with a higher degree of accuracy.

2. Longitudinal conduction analysis

Fig. 1 shows a cross section of the channel. The effects of longitudinal heat conduction in the wall can be characterised by the axial conduction number M introduced by Peterson [6]. In the study reported in Maranzana et al. [10], axial conduction was found to be negligible when M was lower than 10^{-2}.

The non-dimensional number M quantifies the relative importance of conduction heat transfer compared to the energy flow carried by the fluid. Assuming that the axial heat flux in the wall is one-dimensional, and assuming that the temperature difference along the wall is the same as the temperature rise of the fluid $T_{\text{bulk-out}} - T_{\text{bulk-in}}$, the axial conduction number M can be written as follows:

$$M = \frac{k_w A_w (T_{\text{bulk-out}} - T_{\text{bulk-in}})/L}{m c_p (T_{\text{bulk-out}} - T_{\text{bulk-in}})} = 4 \frac{A_w}{A_1} \frac{k_w}{k_f} \frac{1}{Re\,Pr} \tag{1}$$

where L is the channel length, k_w and k_f are the wall and fluid thermal conductivity, A_w is the wall cross section (i.e. the grey area in Fig. 1) and $A_1 = 2(P + e_f)L$ is the wall/fluid interface area of the channel (not considering the presence of the fins in the present case), here called primary channel area. P is the channel width and e_f is the channel thickness, as shown in Fig. 1. The Reynolds number in Eq. (1) is based on the hydraulic diameter of the channel computed without considering the presence of the fins, i.e. $D_h^* = 2Pe_f/(P + e_f)$ (for the studied case, $D_h^* \approx 0.012$ m).

The present test section is made of aluminium, so that the wall thermal conductivity k_w is very high and the axial conduction number M can be moderately high. This study covers operating conditions with a range of variation of the axial conduction number M from 0.003 to 0.03, so from negligible to significant longitudinal conduction effect in accordance with Maranzana et al. [10].

Fig. 2 shows a longitudinal section of a basic piece of heat exchanger divided in wall and fluid cells as well as the 1D heat fluxes.

The elementary hypothesis in data reduction is that heat losses to the environment and longitudinal conduction are negligible so that the local heat flux density entering the fluid and exiting the heaters is the same and uniform (i.e. q_h). Under these assumptions, the energy balance at the fluid cell leads to the following equations:

$$P q_h = P_1 \left(1 + \eta \frac{A_2}{A_1}\right) h (T_w - T_{\text{bulk}}) \tag{2}$$

$$P q_h = m c_p \frac{dT_{\text{bulk}}}{dz} \tag{3}$$

where $P_1 = P + e_f$ is half the perimeter of the channel not considering the fins, η is the fin effectiveness, $A_2 = 2(fP - 1)e_f L$ is the fins area (here called secondary channel area), and f is the number of fins per meter of channel width.

The local HTC (h) can then be obtained from Eq. (2):

$$h = \frac{q_h}{T_w - T_{\text{bulk}}} \frac{1}{1 + \eta (A_2/A_1)} \frac{P}{P_1} \tag{4}$$

Eq. (3) shows that in the case of negligible longitudinal conduction effects and when the fluid specific heat c_p is not temperature-dependent, the fluid bulk temperature T_{bulk} changes linearly along the channel; thus, its local value can be computed by a linear interpolation between the inlet and outlet measurements.

Alternatively, an analysis, considering longitudinal conduction as well, can be obtained for the situation depicted in Fig. 2 by conducting a 1D energy balance in a similar way as the one developed in Mills [11] for a two-stream heat exchanger.

The energy conservation principle across the wall cell of length Δz leads to the following equation:

$$P \Delta z q_h - k_w \frac{A_w}{2} \frac{dT_w}{dz}\bigg|_z = P_1 \left(1 + \eta \frac{A_2}{A_1}\right) \Delta z h (T_w - T_{\text{bulk}}) - k_w \frac{A_w}{2} \frac{dT_w}{dz}\bigg|_{z+\Delta z} \tag{5}$$

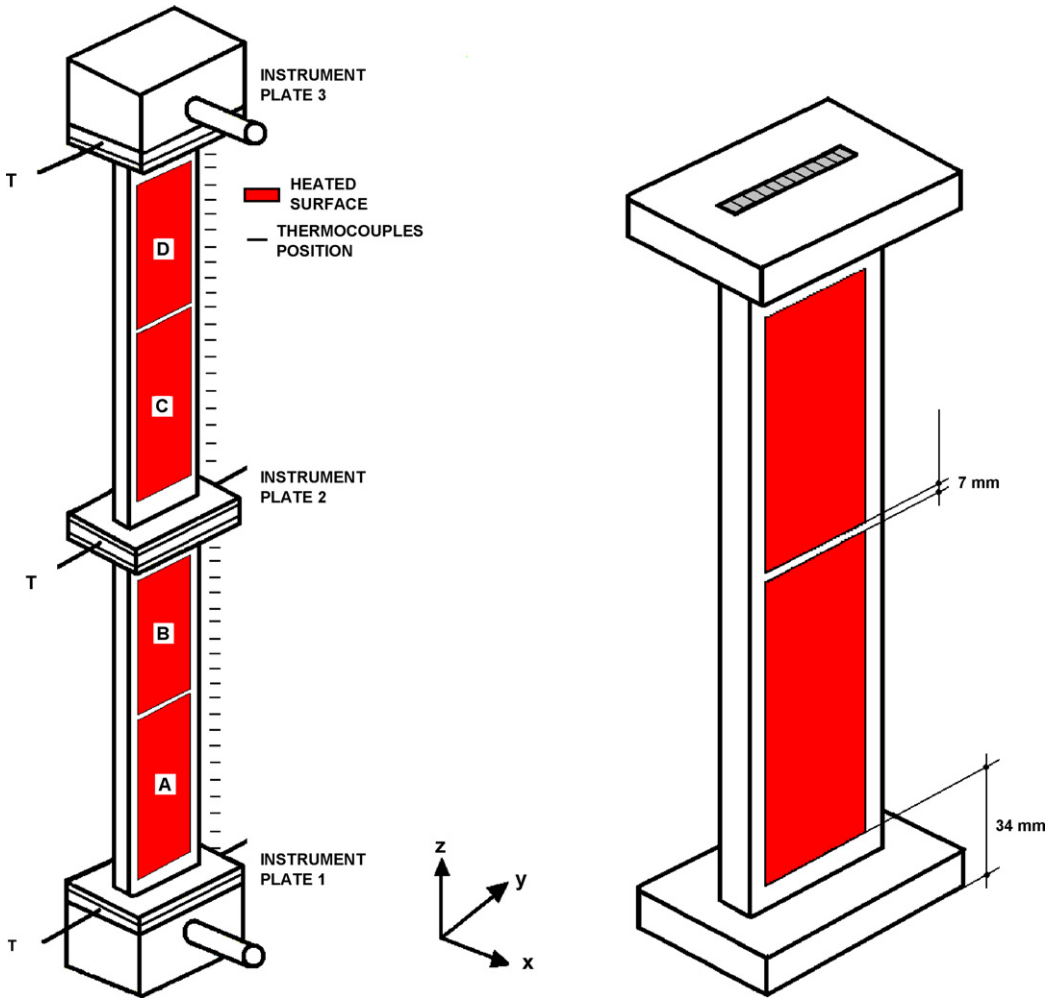

Fig. 3. Test section with position of thermocouples, channel zones and instrument plates (on the left) and half of the test section with indication of the heated areas (on the right).

which, when $\Delta z \to 0$ leads to the following ODE:

$$Pq_h = P_1\left(1+\eta\frac{A_2}{A_1}\right)h(T_w - T_{\text{bulk}}) - k_w\frac{A_w}{2}\frac{d^2T_w}{dz^2} \tag{6}$$

The term on the right-hand side of Eq. (6) represents the effect of longitudinal conduction and is the one not considered in the elementary data reduction procedure as compared to Eq. (2). Now, the value of the local HTC can be obtained from Eq. (6) as:

$$h = \frac{q_h}{T_w - T_{\text{bulk}}}\frac{1}{1+\eta(A_2/A_1)}\frac{P}{P_1}\left(1+\frac{\frac{d}{dz}(k_w A_w\frac{dT_w}{dz})}{2Pq_h}\right) \tag{7}$$

The term in Eq. (7) not present in Eq. (4) explicitly represents the effect of the longitudinal conduction on the local HTC evaluation as it alters the spatial distribution of the heat flux density reaching the fluid. The relevance of the longitudinal conduction effect depends on the ratio between the first derivative in z direction of the longitudinal heat flow rate $k_w A_w(dT_w/dz)$, and double the electrical heater mat width multiplied by electrical heat flux ($2Pq_h$). A uniform temperature variation along the test section from bottom to top would have no influence on the distribution of the local heat flux reaching the fluid since the derivative in z direction would be zero.

However, the longitudinal heat flux cannot be uniform all along the test section since part of the heat is conducted longitudinally to places where there is no electrical heat and, because of this effect, the fluid bulk temperature does not vary linearly in the longitudinal direction.

Potential error in the HTC determination not only depends on the corresponding errors in the measurement of wall temperature, fluid temperature and overall applied power, but also on (a) the interpolation method employed to evaluate the local value of fluid temperature T_{bulk}, (b) the evaluation of the first derivative in z direction of the longitudinal heat flow rate in Eq. (7) and (c) the amount of heat loss to the environment.

Additionally, it should be considered that the heat distribution through the walls and to the fluid is actually a 3D problem, so the 1D balance employed to obtain Eq. (7) is a simplification of what truly takes place.

A full 3D conduction study of the test section was performed on several experimental test cases first to characterise the above-described phenomena and then to assess their influence on the local HTC evaluation.

3. Test section description

The test rig is mainly composed of a pressurising loop and a circulating loop which ensure independent metering of the fluid flow rate and absolute pressure as well as the setting of the inlet conditions. The test fluid is *n*-pentane.

Fig. 3 shows on the left a simplified scheme of the test section geometry. The test section consists of two parts: bottom and top separated by the intermediate instrument plate. The channel inside the test section has four zones (A, B, C, D in Fig. 3) measuring approximately 0.3 m in length each. The test section is made of

Table 1
Approximate characteristics of the different test section zones.

Test section zone	Fin thickness/height (mm)	D_h (mm)	f (fins per meter)	Fin pad
D	0.2/6.5	2	700	Long serration length (25 mm)
C	0.2/6.5	2	700	Long serration length (25 mm)
B	0.2/7	2	700	Short serration length (3 mm)
A	0.2/7	2	700	Perforated

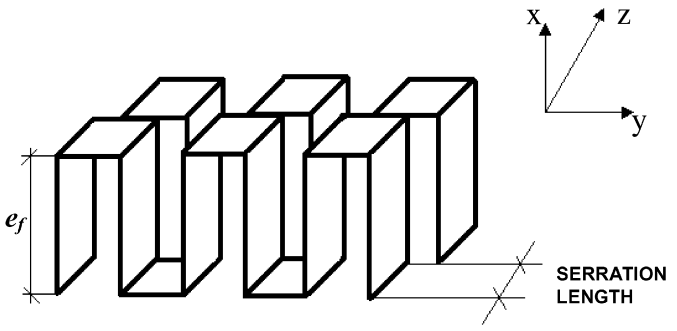

Fig. 4. Illustration of the layout of the serrated fins.

aluminium and the wall thickness is $e_w = 0.007$ m. Inside each zone a particular internal fin pad made of aluminium is brazed to the walls. The dimensions of the fluid channel are approximately 0.075 m × 0.007 m.

Table 1 summarises the main characteristics of the different zones of the studied test section. Channel A has perforated fins, while B, C and D have serrated fins. Channel B has a short serration length. Channels C and D are identical and have long serration length. The hydraulic diameter of the channels taking into account the presence of the fins ($D_h = 2(1/f)e_f/((1/f) + e_f)$) is around 0.002 m for all the zones. An illustration of the layout of the serrated fins is shown in Fig. 4.

The wall temperature is measured all along the test section, with thermocouples placed in thermowells situated at both sides of the fluid channel, as indicated in Fig. 1, totalling 80 readings from bottom to top (see Fig. 3). The thermowells consisted of a square passage of 1.5 mm side going across the test section from side to side in the transversal direction (Fig. 1). The remaining aluminium layer between the passages and the fluid channel is 1 mm thick. The passages were first filled in with a high conductive paste and then, the thermocouple wires (1.1 mm) were inserted into the holes in a way that the measuring tip of the thermocouple was approximately located at the middle of the passage.

Due to the presence of the fins it is not possible to measure the fluid temperature all along the test section. The pentane temperature can only be measured at three instrument plates, allowing the measurement of temperature and pressure, situated respectively at the inlet, middle and outlet of the test section (see Fig. 3), and therefore it must be interpolated at the positions corresponding to wall thermocouples in order to evaluate the local temperature difference between the wall and the fluid ($T_w - T_{\text{bulk}}$) in Eq. (7). The fluid temperature is measured with thermocouples made from the same wire than the wall thermocouples, inserted in long thermowells fully immersed in the fluid flow.

All the thermocouples are T-type (copper/constantan), all made from the same wire in order to reduce the scatter among temperature readings, which was experimentally checked to be lower than 0.03 K. The temperature is measured against a reference cold junction; the temperature of the cold junction, in turn, is measured with an RTD, and is calibrated to provide an accuracy of ±0.1 K over the entire temperature range.

Mass flow rate is measured by a Coriolis effect mass flowmeter, with an accuracy of ±0.6% at $m = 0.011$ kg/s, up to ±0.2% at $m = 0.166$ kg/s.

Fig. 3 indicates the position of the electrical heater mats which are clamped to the sides of the test section by means of 0.01 m thick aluminium plates, with a Teflon™ sheet in-between them to eliminate air spaces. Heaters are 0.0003 m thick. The filament has a serpentine pattern with a special design allowing for a nearly uniform surface power density. The heated surface has the same width (i.e. P) as the channel, as shown in Fig. 1, but it does not cover the entire length of each zone, as shown in Fig. 3. Considering the effective heating area, there is a distance of 0.007 m between the two thermofoils and 0.034 m between the heat mat and the channel inlet or outlet. Heating power is measured separately for each of the four zones A, B, C and D by power transducers with an accuracy of 0.3%. Maximum total heating power is 12,000 W, corresponding to about 80,000 W/m^2 heat flux density. Wall temperature is measured only at the directly heated areas.

A good outer insulation of the test section is essential, since data reduction is based on the assumption of negligible heat loss to the environment. Therefore the entire test section is insulated by a number of layers of elastomeric material followed by a final layer of glass fibre with a low emissivity outer surface. Furthermore, the test section is housed inside a metal box filled with nitrogen to eliminate any possibility of explosion.

4. Numerical and experimental study

A short series of experimental tests were carried out in order to study the heat conduction through the solid part of the test section and the distribution of the heat flux to the fluid.

The maximum range of possible mass flow rates and temperatures was covered. The maximum flow rate was limited by the maximum speed of the circulation pump whereas the minimum was mainly limited by certain instability of operation of the pump at lower speeds and by the loss of accuracy of the mass flowmeter at lower flow rates. As a result, the study covered a wide range of operation with mass velocities G ranging from 20 to 200 kg/m^2 s.

The Reynolds number evaluated with the hydraulic diameter of the channel with fins $D_h = 2(1/f)e_f/((1/f) + e_f)$ ranges from $Re = 200$ up to $Re = 2000$. Channels with offset strip fins induce a considerable degree of turbulence since very low Reynolds numbers. The Re range covered in this study fall into the transition regime of these channel geometries which typically present a very smooth transition from laminar to turbulent flow with monotone variation of the HTC and friction factor (see for instance Kays and London [12]).

Maximum wall temperature was limited to 110 °C for safety reasons.

Then, numerical simulations of the heat conduction in all the solid parts were conducted in order to better study the heat distribution all along the test section and into the fluid. A 3D numerical model of the test section was developed by means of FLUENT 6.1 code [13]. The preprocessor employed for geometry modelling and mesh generation was GAMBIT 2.0. Only one-fourth of the test section was considered for the study given the symmetry of the problem. Elements were hexahedrons or prisms. The initial mesh had some 165,000 cells, but successive adaptations led to up to 600,000 cells.

Since the study was intended to specifically capture all those geometrical details which could influence heat conduction, all metal parts (aluminium exchanger, instrument plates, inlet and outlet headers, plates to clamp the heaters, steel screws) and Teflon gaskets (in-between parts of the test section and instrument

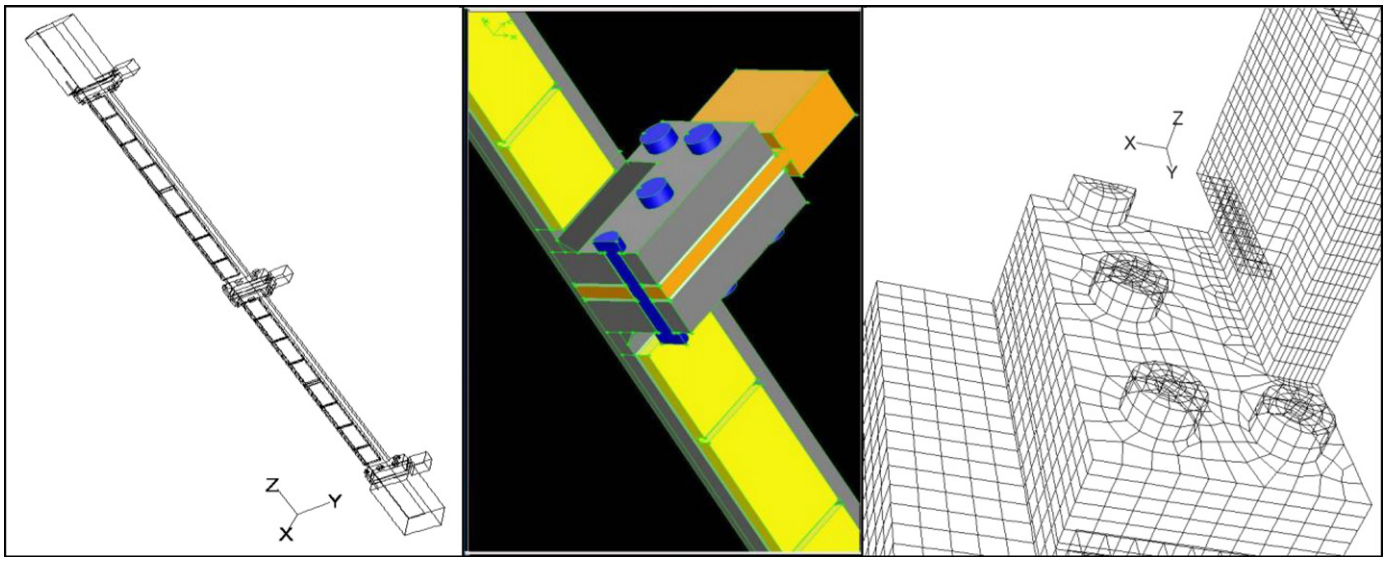

Fig. 5. Computational mesh of the test section.

plates, and inlet/outlet headers as well as between the clamping plates and the heater mats) were modelled. Fig. 5 shows some images of the numerical mesh employed.

The purpose of the numerical study was not to compute the fluid flow but the heat conduction along the test section in order to analyse the heat distribution along the test section and into the fluid. Therefore, the fluid flow modelling was just employed as a way of generating the boundary condition at the wall of the test section by imposing the HTC and the fluid temperature found in the experiments. Turbulent modelling was used in the numerical simulation for the flow field in order to be able to generate a uniform transversal temperature profile, which in reality is promoted by the offset-strip fins. Since the local HTC at the interface between fluid and solid is computed by the code (FLUENT) as a function of the turbulent kinetic energy k, the turbulent dissipation rate ε and the pentane thermal conductivity k_f, uniform values for those parameters where manually adjusted at each of the four zones A, B, C and D in order to reproduce the experimental fluid and wall temperature profiles. In this way, the heat transfer to the fluid found in the experiments was reproduced and the numerical simulation was focused only on the heat conduction problem in the solid parts.

This kind of numerical study can be easily performed with any CFD software package, allowing the detailed analysis of the 3D heat conduction along the test section with low computational effort if experimental results of the fluid and wall temperatures are available.

It should be pointed out that in order to adequately reproduce the fluid temperature evolution it is important to implement in the CFD software an accurate evaluation of the fluid properties, especially, of the specific heat c_p which is temperature dependent.

The electrical mats (heaters) were not explicitly meshed since they are actually very thin, but they were considered in the calculations by setting the desired heat generation rate at the corresponding surfaces.

The external insulation material was not meshed. The heat loss through the insulation from the surface of the test section was considered by a simple 1D model taking into account the thermal resistances corresponding to the thermal insulation first, and then, to the convection to the air inside the box and the radiation to the box wall. For the air temperature inside the box and the box wall temperature, the measured values from the experiments were employed.

5. Results and discussion

5.1. Fluid and wall temperature

Examples of calculated pentane bulk temperature T_{bulk} and calculated wall temperature T_w for different flow rates are shown in the graphs in Fig. 6(a)–(d), along with the experimental data. The heating power per electrical mat applied to that sample of results was around $P_{\text{htr}} = 375$ W.

One can observe several steps on the wall temperature at the inlet, middle and outlet sections corresponding to the high thermal resistance that the gasket in between the aluminium pieces imposes on the heat flux. Those thermal barriers are in some way bypassed by the thermal bridge formed by the steel screws. In any case, the thermal conductivity of the screws is quite low, and the bridge effect is quite small. Those actual details of the construction of the test section have a great influence on the global thermal conductance of the system. This is the reason why the analysis has taken into consideration all possible details.

Notice that the calculated wall temperature at the inlet and outlet of the test section is lower than the fluid temperature. This result is consistent with the fact that in those parts the fluid tends to cool down. Since in those areas there are no fins and the HTC is comparatively low, the temperature difference between the fluid and the wall is quite high. Furthermore, this difference is also dependent on heat loss through the outer insulation which is in turn dependent on the temperature difference between the fluid and the environment, as shown in Fig. 6(a).

Qualitatively, the perforated fins of zone A induce the least turbulent flow, so that the HTC is the lowest, and the difference between the wall and bulk temperatures the highest. This temperature difference is much lower in zone B, where the fins has a very short serration length and induce very high HTC.

The graphs in Fig. 6(a)–(d) include the fluid temperature line indicated as “theoretical bulk temperature” which is estimated, following the elementary data reduction procedure, from the measured values of the fluid temperature at the inlet, middle and top instrument plates, assuming that the heat is applied uniformly along the directly heated areas, without any additional heat gain or loss along the other parts of the channel. The “theoretical bulk temperature” is constant in the unheated zones and changes linearly in the directly heated zones.

Fig. 6(a) shows that this estimated fluid temperature significantly differs from the calculated values, and that the error is rela-

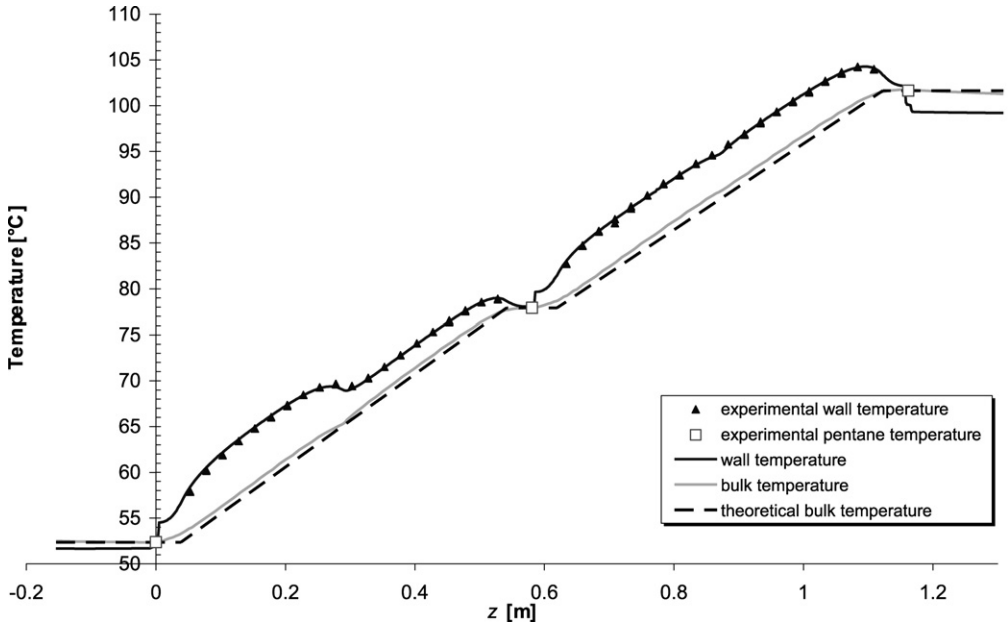

(a) $m = 0.0113$ kg/s, $P_{\text{htr}} = 373.1$ W, $M = 0.03$

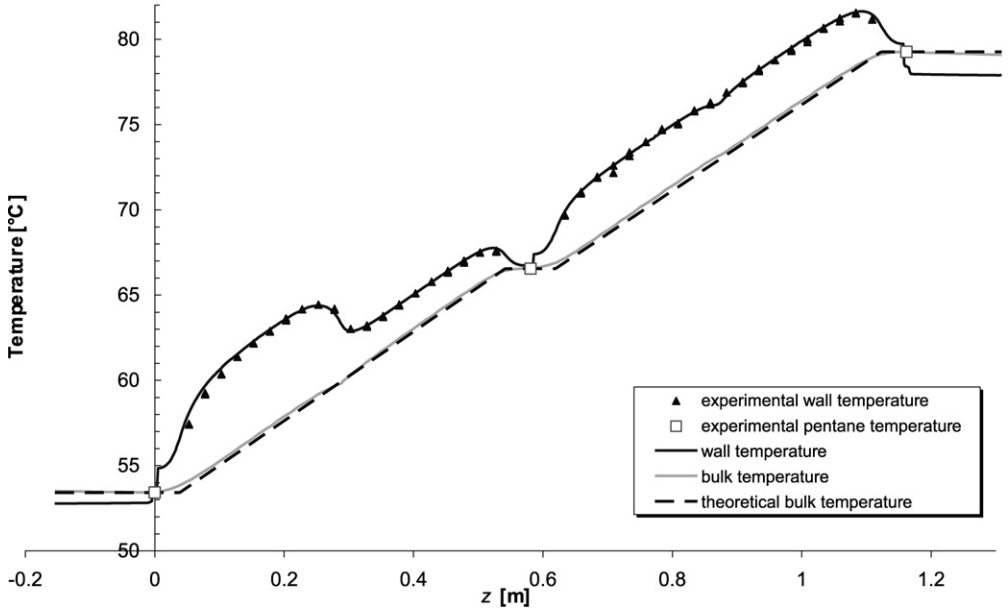

(b) $m = 0.0224$ kg/s, $P_{\text{htr}} = 375.1$ W, $M = 0.015$

Fig. 6. Computed and experimental wall and fluid temperature evolution along the test section.

tively high in comparison with the temperature difference between the wall and the fluid $T_w - T_{\text{bulk}}$. In particular, the computed bulk temperature is higher than the "theoretical bulk temperature". This is due to the longitudinal conduction phenomenon: when pentane reaches the heating resistance edge, its temperature has already been increased by the heat transferred to the fluid at the entrance region through the wall. Similar temperature behaviour can be observed as well in the analyses by Herwig and Hausner [2], Fedorov and Viskanta [3], Li et al. [5], Tiselj et al. [9] and Maranzana et al. [10].

The values of the axial conduction number M are reported in each graph caption. Neglecting heat losses to the environment, the convective heat flow rate transferred to the fluid has been assumed equal to the total heating power; while the axial heat transfer in the wall has been estimated as follows, assuming that the heat transfer is one-dimensional and the temperature rise along the wall is the same as the temperature rise in the fluid:

$$\frac{k_w A_w (T_{\text{bulk-out}} - T_{\text{bulk-in}})}{L} \tag{8}$$

L being the test section length.

As commented above, Maranzana et al. [10] reported that the effect of axial conduction could be assumed negligible when the M number dropped lower than 10^{-2}. This value could also be accepted in the case of the present analysis.

As Eq. (7) indicates, the error in the estimation of the temperature difference between the wall and the fluid $T_w - T_{\text{bulk}}$ is transferred to the error in the evaluation of the local HTC. This error can be quite high and will be more pronounced at the zones with the highest HTC since the temperature difference between the wall and fluid are the lowest, as well as at low mass flow rates

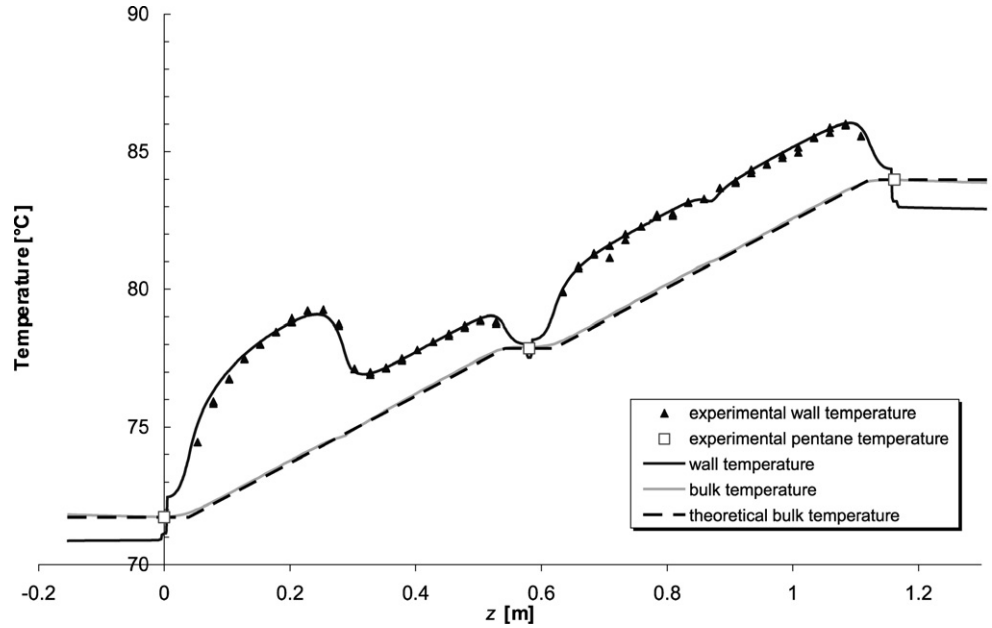

(c) $m = 0.0455$ kg/s, $P_{\text{htr}} = 372.2$ W, $M = 0.007$

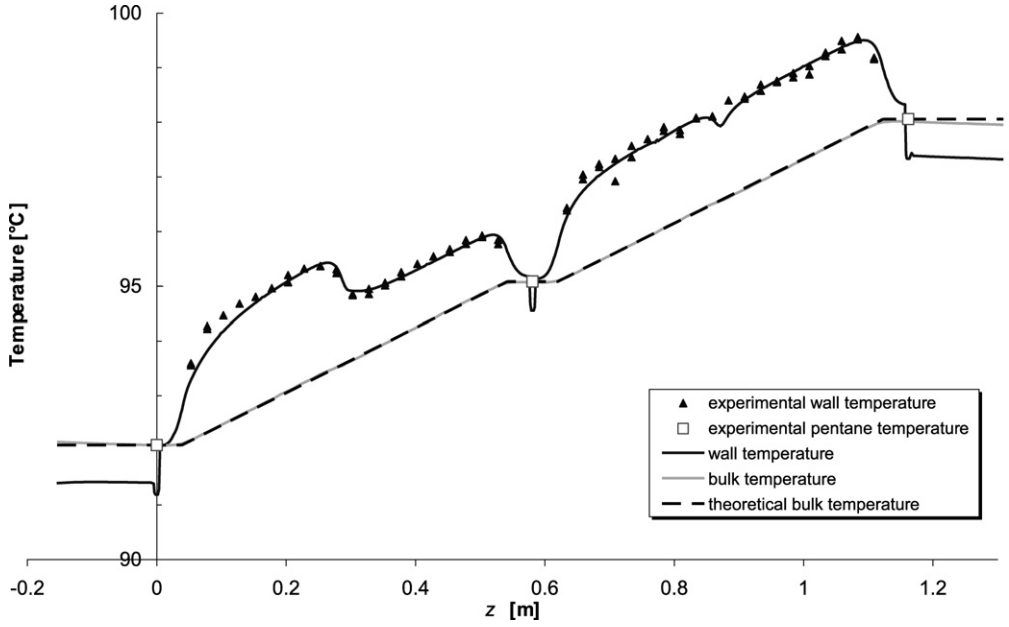

(d) $m = 0.0915$ kg/s, $P_{\text{htr}} = 377.6$ W, $M = 0.003$

Fig. 6 (*continued*).

when the absolute error is the highest. The relative error in computing $T_w - T_{\text{bulk}}$ by using the "theoretical bulk temperature", and in consequence in the HTC evaluation, can reach 30% in zone B at flow rate $m = 0.011$ kg/s, while at $m = 0.092$ kg/s it becomes about 1–2%.

Therefore, the uncertainty in the estimation of the fluid temperature evolution could be significant, leading to a considerable error on the HTC evaluation. The lower the mass flow rate, the higher the error, as reported also in the studies by Li et al. [5] as well as by Maranzana et al. [10].

As easily observed in Fig. 6, the difference between the wall and bulk temperatures is not constant throughout each zone, presenting a strong effect at the beginning and end of each zone. This effect clearly extends to the two first and two last thermocouple readings of each zone, especially at the bottom, middle and top, but also at the change between zones A and B. Initially, this could be interpreted as a "channel entrance effect", however, this is not the case since a constant HTC was imposed all along the zones A, B, C and D, so that the observed effect is attributed to the longitudinal conduction phenomenon.

5.2. Longitudinal heat flux and heat flux transferred to the fluid

Eq. (7) shows that, in addition to the possible error in the estimation of the local temperature difference between the wall and the fluid $T_w - T_{\text{bulk}}$, the effect of the longitudinal conduction on the HTC evaluation also depends on the alteration of the spatial distribution of the local heat flux reaching the fluid, given by:

$$1 + \frac{\frac{d}{dz}\left(k_w A_w \frac{dT_w}{dz}\right)}{2Pq_h} \tag{9}$$

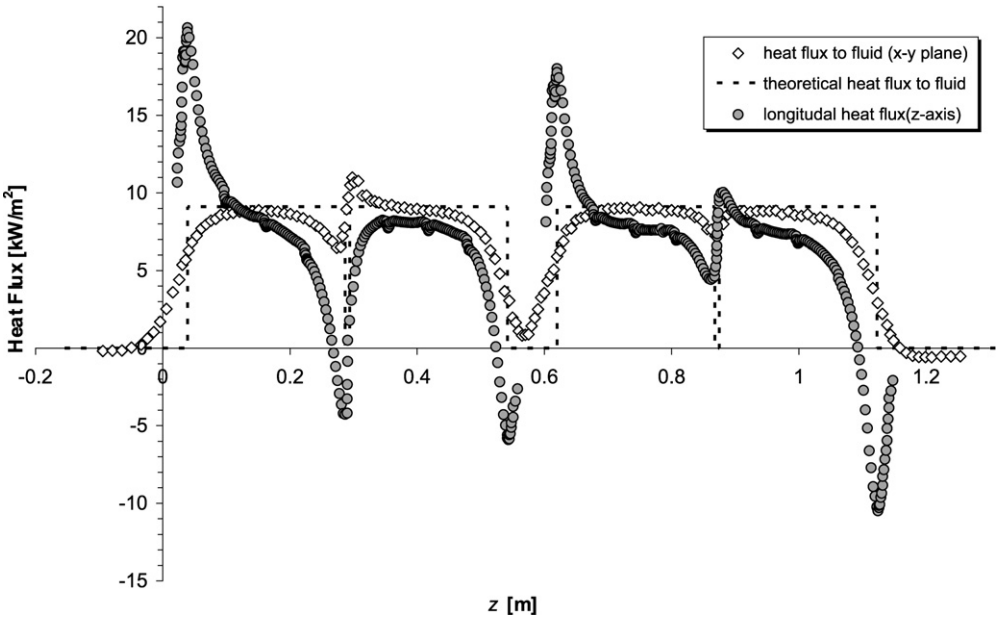

(a) $m = 0.0113$ kg/s, $P_{\text{htr}} = 373.1$ W, $T_{\text{bulk-out}} - T_{\text{bulk-in}} = 49$ K, $k_w(T_{\text{bulk-out}} - T_{\text{bulk-in}})/L = 7000$ W/m^2

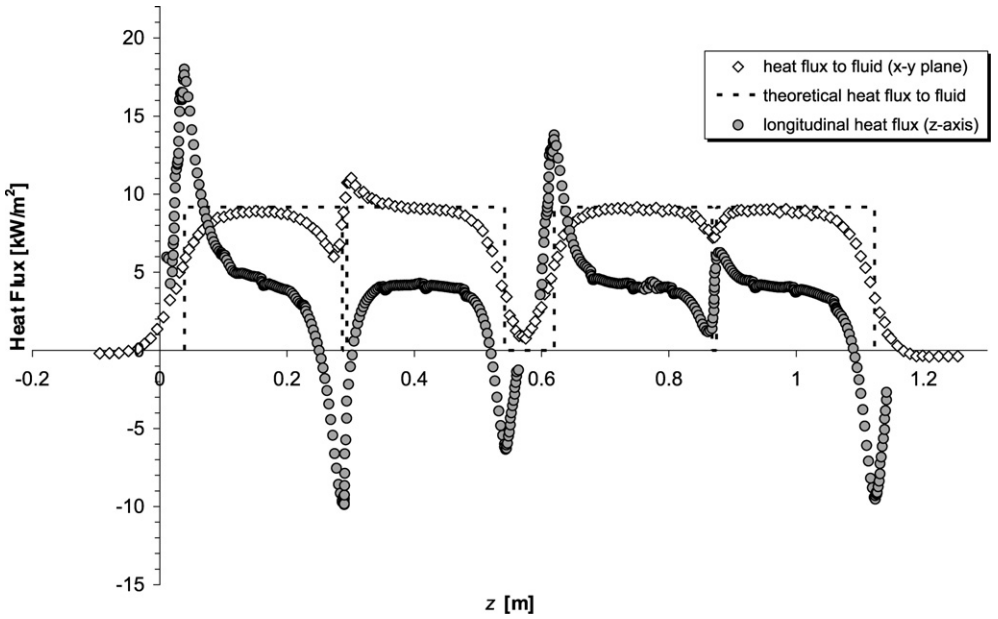

(b) $m = 0.0224$ kg/s, $P_{\text{htr}} = 375.1$ W, $T_{\text{bulk-out}} - T_{\text{bulk-in}} = 26$ K, $k_w(T_{\text{bulk-out}} - T_{\text{bulk-in}})/L = 4000$ W/m^2

Fig. 7. Computed longitudinal heat flux and heat flux transferred to the fluid.

Actually, part of the electrical heat is dissipated to the environment and therefore the reference heat flux density in the above expression should be the heat flux density gained by the aluminium wall instead of the electrical one q_h. Numerical simulations were performed to compute the heat losses for a quite large set of operating conditions. As expected, computed heat losses were small, except at low flow rates and high heating powers. The overall heat losses totalled 2% of the applied power for the sample of conditions considered in the present paper.

The following terms have been computed from the results of the numerical simulation and reported in the graphs in Fig. 7(a)–(d) for the same sample of conditions as in Fig. 6:

Longitudinal conduction heat flux density:

$$k_w \frac{dT_w}{dz} \tag{10}$$

Heat flux density to the fluid:

$$\frac{mc_p}{2P_1}\frac{dT_{\text{bulk}}}{dz} \tag{11}$$

The "theoretical heat flux to the fluid" in Fig. 7(a)–(d) was calculated under the assumptions of negligible heat loss to the environment and negligible longitudinal heat conduction effect. The longitudinal heat flux was considered positive when it moves in the direction opposite to the fluid flow. Each graph caption includes the value of the averaged longitudinal heat flux density along the test section:

$$\frac{k_w(T_{\text{bulk-out}} - T_{\text{bulk-in}})}{L} \tag{12}$$

The first observation from Fig. 7 is that the longitudinal conduction heat flux density presents a huge variation along each zone. This variation would, of course, lead to high derivative values and

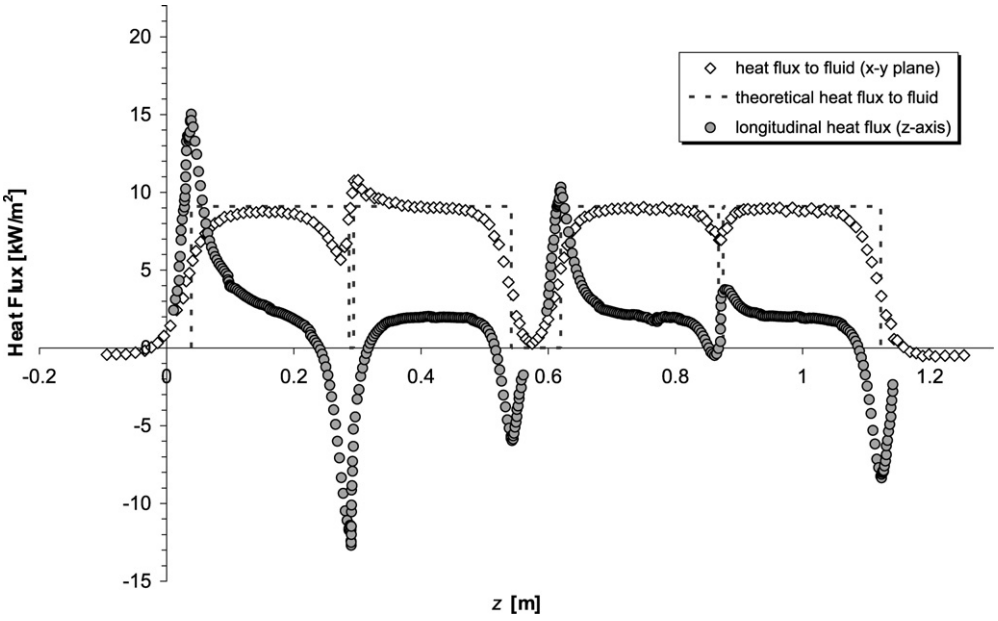

(c) $m = 0.0455$ kg/s, $P_{\text{htr}} = 372.2$ W, $T_{\text{bulk-out}} - T_{\text{bulk-in}} = 12.3$ K, $k_w(T_{\text{bulk-out}} - T_{\text{bulk-in}})/L = 1800$ W/m^2

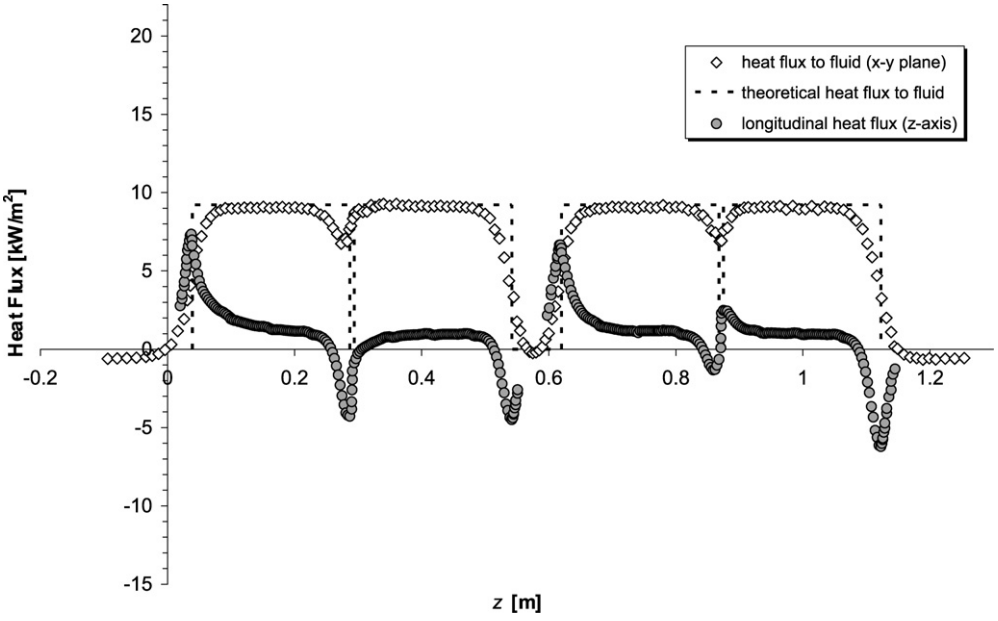

(d) $m = 0.0915$ kg/s, $P_{\text{htr}} = 377.6$ W, $T_{\text{bulk-out}} - T_{\text{bulk-in}} = 6$ K, $k_w(T_{\text{bulk-out}} - T_{\text{bulk-in}})/L = 800$ W/m^2

Fig. 7 (*continued*).

therefore to a strong influence on the HTC evaluation. Notice that the central region at each zone approaches the average value defined in expression (12).

In general, one can observe a high positive peak of the longitudinal conduction at the entrance region of each half part of the test section, but also strong negative peaks at the outlet region. The only exception is the jump in between zones C and D.

The net effect of the longitudinal conduction is clearly seen on the curve of the heat flux transferred to the fluid in Fig. 7. As observed, the heat flux transferred to the fluid in the zones of the fins, where the electrical heat is applied, is always lower than the electrical heat flux. The difference between the electrically supplied heat and the heat transferred to the fluid is redistributed, thanks to the longitudinal conduction effect, to all the unheated areas of the test section and, in a small portion, to the environment.

The only exception to this rule is the heat flux at the beginning of zone B, which in certain cases [(a)–(c)] reaches a higher heat flux. This is due to the fact that the thermal resistance to the fluid at zone B is much lower than that at zone A, given the effect of the serration on the fins. This means that a part of the electrical heat applied to zone A escapes from A and goes to B, increasing the heat flux density to the fluid at the entrance region.

The results obtained can be explained by a combination of three different longitudinal conduction phenomena illustrated in Fig. 8.

As a first approximation, the fluid temperature T_{bulk} has a constant slope all along the test section. Wall temperature T_w must follow someway T_{bulk} and its slope, and its temperature gradient in z-direction causes heat conduction from top to bottom. We called this: Phenomenon 1. The general effect of this phenomenon is heat transferred in the direction opposite the fluid flow. The

average value of the heat flux density will be given by expression (12) and therefore will increase with the increase of the applied electrical power and with the decrease of the mass flow rate. Phenomenon 1 will not influence the spatial distribution of the heat flux reaching the fluid, however, it is the main responsible for the fact that when pentane reaches the heating resistance edge its temperature has already been increased by the heat transferred to the fluid at the entrance region through the wall, therefore it is responsible for the possible errors when evaluating the local fluid temperatures by interpolation between the measured values at the inlet, middle and top positions.

At the ends of the two halves of the test section the temperature of the wall is considerably higher than in the neighbouring parts where no heat is applied; therefore, some heat would "escape" through the wall towards the unheated zones. We called this: Phenomenon 2. This phenomenon is not continuous and changes its sign from left to right as indicated in Fig. 8.

Finally, as commented above, the thermal resistance to the fluid at zone B is much lower than at zone A, due to the effect of the serration on the fins, which makes the wall temperature at the end of zone A higher than the wall temperature at the beginning of zone B and, consequently, part of the heat supplied at zone A would go to zone B. We called this: Phenomenon 3.

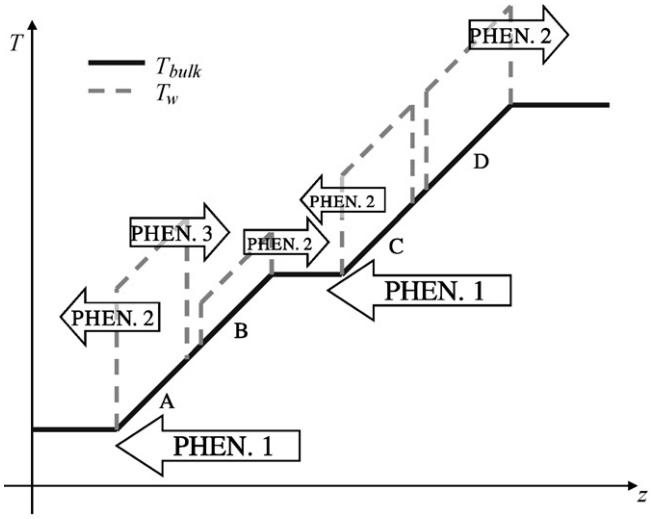

Fig. 8. Illustration of longitudinal conduction phenomena.

Phenomena 2 and 3 influence the spatial distribution of the heat flux density reaching the fluid and are responsible for the alteration of the difference between the wall and bulk temperatures at the beginning and end of each zone. For the analysed test section, these effects clearly extend to the two first and two last thermocouple readings of each zone and may imply the rejection of 10–20% of the experimental data.

Figs. 9 and 10 show the values of the difference between the overall heat transfer rate to the fluid along each zone of the channel, obtained from the numerical simulation results, between zones C and D, and between zones A and B, respectively. They are obtained at different flow rates ($m = 0.011$ kg/s, $m = 0.022$ kg/s, $m = 0.044$ kg/s and $m = 0.092$ kg/s), different fluid inlet temperatures (from $T_{\text{bulk-in}} = 30\,^{\circ}\text{C}$ up to $T_{\text{bulk-in}} = 85\,^{\circ}\text{C}$) and different applied electrical power (from $P_{\text{htr}} = 185$ W up to $P_{\text{htr}} = 2000$ W).

Fig. 9 shows that the overall heat flow rate reaching zone C is always higher than that reaching zone D and that the difference turns out to be linear and mainly dependent on the value of the fluid temperature rise $T_{\text{bulk-out}} - T_{\text{bulk-in}}$. The strong linear dependency indicates that the effect can be mainly characterised by phenomenon 1: sector C lets some heat escape towards the central instrument plate and gets some heat from sector D, while sector D cannot receive heat from above and even loses a portion of it to the upper part of the test section.

Fig. 10 shows that the combination of phenomena leading to the obtained difference between the heat flow rate transferred to the fluid zones A and B is more complex, because all three phenomena observed act together in this case. The results show that in general the heat reaching zone B is higher than that reaching zone A, and this means that in general phenomenon 3 is more relevant than phenomenon 1. However, at $m = 0.011$ kg/s, when $T_{\text{bulk-out}} - T_{\text{bulk-in}}$ is the highest, phenomenon 1 seems to be almost as relevant as phenomenon 3, and they compensate each other. The difference between the overall heat transferred to the fluid is the highest at $m = 0.044$ kg/s, because in this situation phenomenon 3 is very strong, while phenomenon 1 is weak given the small fluid temperature rise.

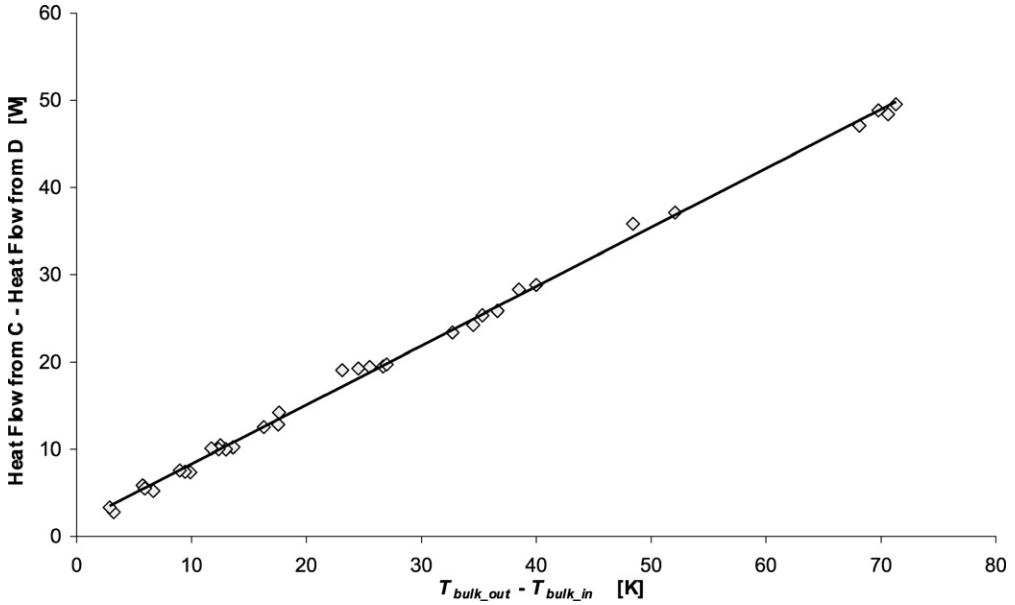

Fig. 9. Difference of the overall heat flow transferred to the fluid between zones C and D.

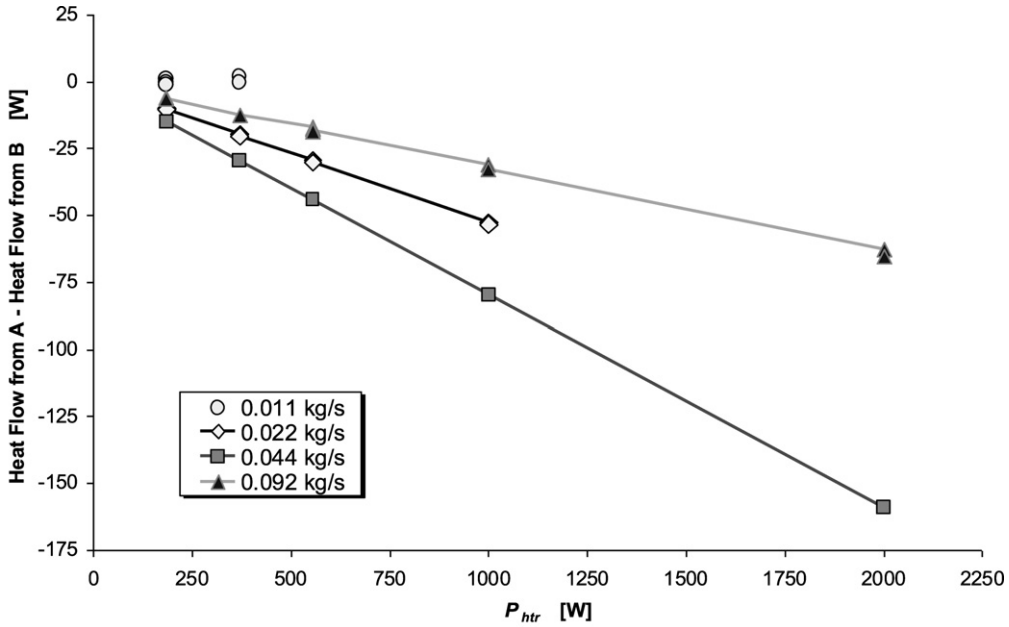

Fig. 10. Difference of the overall heat flow transferred to the fluid between zones A and B.

6. Conclusions

A detailed experimental and numerical analysis was performed to evaluate the effect of longitudinal heat conduction on the local heat transfer coefficient (HTC) experimental determination, through the estimation of the heat flux and temperature distributions all along the aluminium test section.

In the experimental set-up, electrical resistances, whose design assures a uniform power density, are used to heat the fluid stream; wall temperature is measured by numerous thermocouples inserted all along the wall, while fluid temperature is measured at the inlet and outlet, as well as in the middle of the test section.

The present study clearly shows that the elementary data reduction methodology, assuming negligible longitudinal conduction effects, can be far from reality for the employed test section and can lead to important errors in the estimated values of the HTC at the inlet and outlet regions of each zone.

Three different longitudinal heat conduction phenomena were identified as the cause of the uneven heat distribution along the test section:

Phenomenon 1 is due to the fluid temperature rise along the test section, which produces a longitudinal gradient of the temperature along the wall and thus heat conduction in the direction opposite the fluid flow.

Phenomenon 2 is due to the presence of heated and non-heated zones, thus appears at the edges of each heated part of the test section where the electrically supplied heat is redistributed through the wall to the unheated areas.

Phenomenon 3 is due to the stepwise non-uniformity in the distribution of the HTC, induced by the discontinuity of the fin geometry along the channel; because of this phenomenon, a part of the electrical heat applied to the lower HTC zones "escapes" towards the higher HTC zones, increasing the local heat flux density to the fluid at the entrance region.

These three phenomena act in combination producing an imbalance between the electrical heat flux density and the local heat flux density actually transferred to the fluid. This effect is negligible at the central part of each heated zone, but, in the cases reported, it is clearly present at the two first and two last thermocouple readings of each zone and may imply the rejection of 10–20% of the experimental data. Additionally, the longitudinal conduction makes some heat go to the fluid at the inlet area of the test section, producing an increase in the fluid temperature at the inlet, which can be significant when compared with the characteristic temperature difference between the wall and the fluid; this uncertainty on the estimation of the fluid temperature significantly increases the HTC evaluation uncertainty, especially at low flow rates.

Therefore, the data reduction procedure must always include an estimation of longitudinal heat conduction.

Acknowledgements

This research is related with the experimental estimation of Heat Transfer Coefficients of boiling hydrocarbons through characteristic channels of compact heat exchangers, performed at the *Universidad Politécnica de Valencia* (Spain) for HTFS AspenTech Ltd. (U.K.). The authors wish to express their most sincere gratitude to HTFS AspenTech Ltd. for their financial and technical support. This research has also been partially funded by "Fondazione Ing. Aldo Gini" at *Università degli Studi di Padova* (Italy).

The authors are grateful to Debra Westall (*Universidad Politécnica de Valencia*) for her linguistic revision of this text.

References

[1] C.P. Tso, S.P. Mahulikar, Experimental verification of the role of Brinkman number in micro-channels using local parameters, Int. J. Heat Mass Transfer 43 (2000) 1837–1849.
[2] H. Herwig, O. Hausner, Critical view on new results in micro-fluid mechanics: an example, Int. J. Heat Mass Transfer 46 (2003) 935–937.
[3] A.G. Fedorov, R. Viskanta, Three-dimensional conjugate heat transfer in the micro-channel heat sink for electronic packaging, Int. J. Heat Mass Transfer 43 (2000) 399–415.
[4] W. Qu, I. Mudawar, Analysis of three-dimensional heat transfer in micro-channel heat sinks, Int. J. Heat Mass Transfer 45 (2002) 3973–3985.
[5] J. Li, G.P. Peterson, P. Cheng, Three-dimensional analysis of the heat transfer in a micro-heat sink with single phase flow, Int. J. Heat Mass Transfer 47 (2004) 4215–4231.
[6] R.B. Peterson, Numerical modelling of conduction effects in microscale counterflow heat exchangers, Microscale Thermophys. Engrg. 3 (1999) 17–30.
[7] K. Kawano, K. Minakami, H. Iwasaki, M. Ishizuka, Development of micro-channel heat exchanging, in: R.A. Nelson Jr., L.W. Swanson, M.V.A. Bianchi, C. Camci (Eds.), Application of Heat Transfer in Equipment, Systems, and Education, HTD-Vol. 361-3/PID-Vol. 3, ASME, New York, 1998, pp. 173–180.

[8] W. Qu, I. Mudawar, Experimental and numerical study of pressure drop and heat transfer in a single-phase micro-channel heat sink, Int. J. Heat Mass Transfer 45 (2002) 2549–2565.
[9] I. Tiselj, G. Hetsroni, B. Mavko, A. Mosyak, E. Pogrebnyak, Z. Segal, Effect of axial conduction on the heat transfer in micro-channels, Int. J. Heat Mass Transfer 47 (2004) 2551–2565.
[10] G. Maranzana, I. Perry, D. Maillet, Mini- and micro-channels: influence of axial conduction in the walls, Int. J. Heat Mass Transfer 47 (2004) 3993–4004.
[11] A.F. Mills, Heat and Mass Transfer, Irwin, Chicago, 1995, pp. 741–743.
[12] W.M. Kays, A.L. London, Compact Heat Exchangers, third ed., Krieger, 1998.
[13] Fluent Inc., 2001. FLUENT 6.0 User's Guide, Lebanon, NH.